JOURNAL OF MATERIALS PROCESSING TECHNOLOGY 200 (2008) 481–482

ELSEVIER

available at www.sciencedirect.com

ScienceDirect

journal homepage: www.elsevier.com/locate/jmatprotec

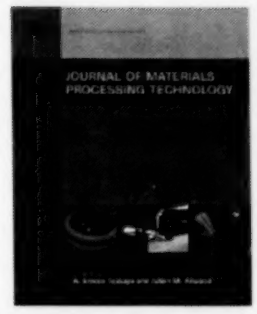

Author Index of Volume 200

Abo-Shosha, M.H., 385
Adhikary, S., 460
Aggarwal, A., 373
Ali, A.I., 271
Ali, F., 316
Almeida, F.A., 126
Almeida, N., 126
Alves Jr., C., 115
Alves, J.L., 416
Amarasinghe, A., 424
Andersson, A., 1
Anvari, S.Z., 312
Ati, A., 410

Balasubramanian, K., 283
Balasubramanian, V., 163
Bastier, A., 25
Bathias, C., 133
Bayraktar, E., 133
Bednarik, V., 265
Benabbas, A., 410
Benedictus, R., 288
Berstad, T., 77
Bing, G.J.A., 176
Bo, C., 405
Bolot, R., 94
Bounar, N., 410
Bozic, D., 106
Bradai, M.A., 410

Cai, L., 158
Cavaliere, P., 364
Chandra, R., 205
Chandramohan, G., 306
Chatterjee, D., 212
Chawla, V., 205
Chen, X., 471
Claypole, T.C., 221
Coddet, C., 94
Costa, B.L.S., 115

Dang Van, K., 25
Davidson, M.J., 283
Davtyan, S.P., 319
de Brito, R.A., 115
Ding, Z., 153
Du, S., 433
Duszczyk, J., 185

Ekered, S., 339
Elangovan, K., 163
El-sayed, Z.M., 385
El-Sonbaty, I.A., 271
Enayati, M.H., 312
Eyercioglu, O., 146

Fahmy, H.M., 385
Fernandes, M.H.F.V., 126
Furu, T., 77

Galvão, N.K.A.M., 115
Gavin, G.P., 38
Gethin, D.T., 221
Gonzalez Garza, M.A., 133
Gu, X., 153

Han, J., 433
Hebeish, A.A., 385
Henriques, E., 250
Hong, H., 12
Hopperstad, O.S., 77

Ibrahim, N.A., 385
Imgrund, P., 259
Iqbal, M.A., 316
Ismail, R., 279

Jain, V.K., 460
Jayaganthan, R., 205
Jovanovic, M.T., 106
Ju, F., 199

Kanca, E., 146
Karimi Taheri, A., 325
Karimzadeh, F., 312
Kayacan, M.C., 347
Kazeminezhad, M., 325
Khan, A.N., 316
Khan, S.H., 316
Khashaba, U.A., 271
Khelifa, M., 71
Kiet Tieu, A., 325
Kong, J.J., 158
Ku, T.-H., 331
Kumar, P., 373

Lademo, O.-G., 77
Lapovok, R., 441
Lermen, R.T., 398
Li, X., 199
Li, Y.X., 471
Liao, C.W., 59
Liao, H., 94
Liljengren, M., 1
Lin, C.-A., 331
Lin, Y.R., 59
Liu, G., 185
Liu, X.Y., 12

Ma, B., 390
Ma, H., 153
Machado, I.G., 398
Maitournam, M.H., 25
Manikya Kanti, K., 300
Matsumura, T., 356
McGuinness, G.B., 38
McKenzie, P.W.J., 441
Mendes, M.W.D., 115
Mendes, R.P.K., 120
Menezes, L.F., 416
Morris, E., 38

Nath, Y., 238
Nemec, A., 265
Northwood, D.O., 433

O'Byrne, J.M., 38
O'Daly, B.J., 38
O'Donnell, R., 441
Oliveira, M.C., 416
Ono, T., 356
Oraon, B., 212
Oudjene, M., 71
Ozbay, E., 146

Padmanabhan, R., 416
Pal, U., 199
Pala, M., 146
Pandey, R.K., 238
Panella, F., 364
Peças, P., 250
Pedersen, K.O., 77
Peng, J., 153
Phillips, C.O., 221
Planche, M.-P., 94

Rajkovic, V., 106
Ridgway, K., 424
Roger, F., 25
Rota, A., 259

Salehi, M., 232
Salehinia, I., 451

Elsevier B.V.
doi:10.1016/S0924-0136(08)00169-6

Salem, A., 232
Salman, Ö., 347
Santos, C., 126
Sargsyan, A.G., 319
Schick, C., 319
Selmy, A.I., 271
Shahani, A.R., 451
Sharman, A.R.C., 424
Silva, R.R.F., 126
Simchi, A., 259
Singh, H., 373
Singh, M., 373
Singh, P., 238
Sinke, J., 288
Slavik, R., 265
Souza Jr., C.F., 115
Souza, R.C., 126
Squillace, A., 364
Srinivasa Rao, P., 300
Su, J.C., 59
Sun, X.J., 471
Suresha, B., 306
Sutradhar, G., 212

Tagore, G.R.N., 283
Tarng, Y.S., 59
Tasdelen, B., 339
Tataryan, A.A., 319
Thilderkvist, P., 1
Timokhina, I., 441
Tonoyan, A.O., 319

Valentina, L.V.O.D., 120
Verran, G.O., 120
Vondruska, M., 265

Wallbank, J., 176
Wang, H., 433
Wei, Q., 405
Weidong, H., 405
Weiqiang, L., 405
Wikblom, T., 339

Xiaohong, W., 405

Yaacob, I.I., 279
Yan, F., 158
Yang, H.F., 158
Ye, H., 12
Yuan, W., 390

Zadpoor, A.A., 288
Zhao, H., 199
Zhaohua, J., 405
Zhou, J., 185
Zhou, M., 158

JOURNAL OF MATERIALS PROCESSING TECHNOLOGY 200 (2008) 483–490

ELSEVIER

available at www.sciencedirect.com

ScienceDirect

journal homepage: www.elsevier.com/locate/jmatprotec

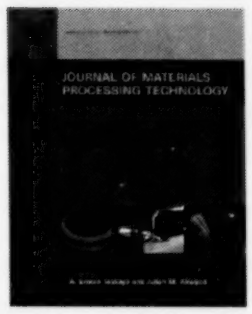

Subject Index of Volume 200

AA6061 alloy
Experimental investigation on flow-forming of AA6061 alloy—A Taguchi approach, 283
AA2219 aluminium alloy
Influences of tool pin profile and welding speed on the formation of friction stir processing zone in AA2219 aluminium alloy, 163
Ablation
High-power low-frequency ultrasound: A review of tissue dissection and ablation in medicine and surgery, 38
Acid resistance
Preparation of geopolymer from fluidized bed combustion bottom ash, 265
Air
Studies on minimum quantity lubrication (MQL) and air cooling at drilling, 339
AISI M35 steel
Structural modifications of M35 steel submitted to thermal gradients in plasma reactor, 115
AISI P-20 tool steel
Optimizing power consumption for CNC turned parts using response surface methodology and Taguchi's technique—A comparative analysis, 373
Al_2O_3 particles
Properties of copper matrix reinforced with various size and amount of Al_2O_3 particles, 106
Aluminium alloys
Influence of texture and grain structure on strain localisation and formability for AlMgSi alloys, 77
Aluminium sheet
Processing and properties of ultrafine-grain aluminium alloy 6111 sheet, 441
Aluminum alloy
White anodized thermal control coating on LY12 aluminum alloy, 405
Aluminum alloys
DOE applied to optimization of aluminum alloy die castings, 120
Anodization
White anodized thermal control coating on LY12 aluminum alloy, 405
Artificial neural networks
Prediction of martensite and austenite start temperatures of the Fe-based shape memory alloys by artificial neural networks, 146
Prediction of bead geometry in pulsed GMA welding using back propagation neural network, 300
Austenite transformation
Prediction of martensite and austenite start temperatures of the Fe-based shape memory alloys by artificial neural networks, 146
Automated visual inspection
Application of the structured illumination method for automated visual inspection of the loudspeaker cones, 59

Bead geometry
Prediction of bead geometry in pulsed GMA welding using back propagation neural network, 300
Bimetals
Microinjection moulding of 316L/17-4PH and 316L/Fe powders for fabrication of magnetic–nonmagnetic bimetals, 259
Blanking
The effect of using a sprung stripper in sheet metal cutting, 176
Bond coat
Study of microstructure, phases and microhardness of metallic coatings deposited by flame thermal spray, 410
Brittle crack
Cutting process of glass with inclined ball end mill, 356
Burr
The effect of using a sprung stripper in sheet metal cutting, 176

Carbon steel
Pearlite determination in plain carbon steel by eddy current method, 316
Central composite design
Fuzzy rule-based prediction of hardness for sintered HSS components, 212
Optimizing power consumption for CNC turned parts using response surface methodology and Taguchi's technique—A comparative analysis, 373
Ceramic
Physical–mechanical, superconducting, thermo-physical properties and interphase phenomena of polymer–ceramic nano-composites, 319
Ceramics
Toughened ZrO_2 ceramics sintered with a La_2O_3-rich glass as additive, 126
Chemical analysis
On the mechanism of material removal in electrochemical spark machining of quartz under different polarity conditions, 460

Elsevier B.V.
doi:10.1016/S0924-0136(08)00170-2

Coating microstructure
Study of microstructure, phases and microhardness of metallic coatings deposited by flame thermal spray, 410
Compacted graphite cast iron
Identification and evaluation of modification level for compacted graphite cast iron, 471
Composite
Physical–mechanical, superconducting, thermo-physical properties and interphase phenomena of polymer–ceramic nano-composites, 319
Compressive strength
Effect of moisture content on extrusion process of kaolinitic–illitic clay in manufacturing of ceramic Raschig ring, 232
Preparation of geopolymer from fluidized bed combustion bottom ash, 265
Computational fluid dynamics
A three-dimensional model of the wire-arc spray process and its experimental validation, 94
Contact and friction
Numerical damage prediction in deep-drawing of sheet metals, 71
Contact pressure
Analysis of wear in deep-drawing process of a cylindrical cup, 451
Convexity index
Prediction of bead geometry in pulsed GMA welding using back propagation neural network, 300
Cotton fabric
Hybrids for finishing cotton fabric with durable handle performance, 385
Cross section
A study on the cross-sectional profile of flat rolled wire, 325
Crosslinker
Hybrids for finishing cotton fabric with durable handle performance, 385
Cryogenic cooling
Optimizing power consumption for CNC turned parts using response surface methodology and Taguchi's technique—A comparative analysis, 373
Cutting
High-power low-frequency ultrasound: A review of tissue dissection and ablation in medicine and surgery, 38
The effect of using a sprung stripper in sheet metal cutting, 176
Cutting process of glass with inclined ball end mill, 356
Development and implementation of a magnetoplasmadynamic thruster for welding and cutting, 398
Cylindrical deep-drawing process
Analysis of wear in deep-drawing process of a cylindrical cup, 451

Damage
Numerical damage prediction in deep-drawing of sheet metals, 71
DD3IMP
Numerical simulation and analysis on the deep drawing of LPG bottles, 416
Deep drawing
Numerical simulation and analysis on the deep drawing of LPG bottles, 416
Deep-drawing
Numerical damage prediction in deep-drawing of sheet metals, 71
Defects
DOE applied to optimization of aluminum alloy die castings, 120
Deformation mechanism–dislocation interaction
A comprehensive study of plastic deformation mechanism of the metallic materials by 'X-ray' computed tomography ('X-ray' CT), 133
Depth of cut
Prediction of surface roughness profiles for milled surfaces using an artificial neural network and fractal geometry approach, 271
Design of experiments
DOE applied to optimization of aluminum alloy die castings, 120
Die casting
DOE applied to optimization of aluminum alloy die castings, 120
Direct etching
Micro-machinability of monocrystal silicon by direct etching using excimer laser, 390
Direct polarity
On the mechanism of material removal in electrochemical spark machining of quartz under different polarity conditions, 460
Draw die radius
Analysis of wear in deep-drawing process of a cylindrical cup, 451
Drilling
Studies on minimum quantity lubrication (MQL) and air cooling at drilling, 339
Tool life and surface integrity aspects when drilling and hole making in Inconel 718, 424
Ductile mode
Cutting process of glass with inclined ball end mill, 356

ECSM
On the mechanism of material removal in electrochemical spark machining of quartz under different polarity conditions, 460
Eddy current
Pearlite determination in plain carbon steel by eddy current method, 316
EDM polishing
Electrical discharge machining using simple and powder-mixed dielectric: The effect of the electrode area in the surface roughness and topography, 250
Elasto-viscoplastic behavior
Analysis of wear in deep-drawing process of a cylindrical cup, 451
Elastoviscoplastic behaviour
Modelling of the residual state of friction stir welded plates, 25
Electrical conductivity
Thin film of bis(ethylenedithio)-tetrathiafulvalene radical salt with Dawson polyoxometalate, 153
Electrical discharge machining
Electrical discharge machining using simple and powder-mixed dielectric: The effect of the electrode area in the surface roughness and topography, 250
Evolutionary programming method for modeling the EDM parameters for roughness, 347
Electrode area
Electrical discharge machining using simple and powder-mixed dielectric: The effect of the electrode area in the surface roughness and topography, 250
Electronic materials
Thin film of bis(ethylenedithio)-tetrathiafulvalene radical salt with Dawson polyoxometalate, 153

Elongational flow properties
Shear and elongational flow properties of thermoplastic polyvinyl alcohol melts with different plasticizer contents and degrees of polymerization, 331
Empirical relations
An efficient thermal analysis for the prediction of minimum film thickness in inlet zone at high speed lubricated cold strip rolling, 238
Emulsion
Studies on minimum quantity lubrication (MQL) and air cooling at drilling, 339
End mill
Cutting process of glass with inclined ball end mill, 356
Equal channel angular processing
Processing and properties of ultrafine-grain aluminium alloy 6111 sheet, 441
Excimer laser
Micro-machinability of monocrystal silicon by direct etching using excimer laser, 390
Extrusion
FE analysis of metal flow and weld seam formation in a porthole die during the extrusion of a magnesium alloy into a square tube and the effect of ram speed on weld strength, 185

Failure
Experimental and numerical study of machined aluminum tailor-made blanks, 288
Fatigue
Effect of welding parameters on mechanical and microstructural properties of AA6082 joints produced by friction stir welding, 364
FE simulation
FE analysis of metal flow and weld seam formation in a porthole die during the extrusion of a magnesium alloy into a square tube and the effect of ram speed on weld strength, 185
Fe-based shape memory alloys
Prediction of martensite and austenite start temperatures of the Fe-based shape memory alloys by artificial neural networks, 146
Feed
Prediction of surface roughness profiles for milled surfaces using an artificial neural network and fractal geometry approach, 271
FEM
Numerical damage prediction in deep-drawing of sheet metals, 71
Finite element analysis of thermal stress in magnetron sputtered Ti coating, 205
FEM modeling
Experimental and numerical study of machined aluminum tailor-made blanks, 288
Femtosecond laser
Study on the microfabrication technique by femtosecond laser two-photon photopolymerization, 158
Fillers
Three-body abrasive wear behaviour of particulate-filled glass–vinyl ester composites, 306
Finishing
Hybrids for finishing cotton fabric with durable handle performance, 385
Finite element simulation
Analysis of wear in deep-drawing process of a cylindrical cup, 451
Flame spraying
Study of microstructure, phases and microhardness of metallic coatings deposited by flame thermal spray, 410
Flow activation energy
Shear and elongational flow properties of thermoplastic polyvinyl alcohol melts with different plasticizer contents and degrees of polymerization, 331
Flow-forming
Experimental investigation on flow-forming of AA6061 alloy—A Taguchi approach, 283
Fluidized bed combustion bottom ash
Preparation of geopolymer from fluidized bed combustion bottom ash, 265
Formability
Experimental evaluation of strains in the tension–compression using a new tool geometry, X-Die, 1
Influence of texture and grain structure on strain localisation and formability for AlMgSi alloys, 77
Forming limit curve
Experimental evaluation of strains in the tension–compression using a new tool geometry, X-Die, 1
Forming limit diagram
Experimental evaluation of strains in the tension–compression using a new tool geometry, X-Die, 1
Fractal geometry approach
Prediction of surface roughness profiles for milled surfaces using an artificial neural network and fractal geometry approach, 271
Fragmentation
High-power low-frequency ultrasound: A review of tissue dissection and ablation in medicine and surgery, 38
Freeze-thaw resistance
Preparation of geopolymer from fluidized bed combustion bottom ash, 265
Friction stir welding
Modelling of the residual state of friction stir welded plates, 25
Influences of tool pin profile and welding speed on the formation of friction stir processing zone in AA2219 aluminium alloy, 163
Effect of welding parameters on mechanical and microstructural properties of AA6082 joints produced by friction stir welding, 364
Fuzzy inference system
Fuzzy rule-based prediction of hardness for sintered HSS components, 212

Genetic expression programming
Evolutionary programming method for modeling the EDM parameters for roughness, 347
Geopolymer
Preparation of geopolymer from fluidized bed combustion bottom ash, 265
Glass
Cutting process of glass with inclined ball end mill, 356
Glass transition
Mechanical properties of polymer films used in in-mould decoration, 221
Glass–vinyl ester composite
Three-body abrasive wear behaviour of particulate-filled glass–vinyl ester composites, 306

Grain structure
Influence of texture and grain structure on strain localisation and formability for AlMgSi alloys, 77

Hand builder
Hybrids for finishing cotton fabric with durable handle performance, 385
High power
High-power low-frequency ultrasound: A review of tissue dissection and ablation in medicine and surgery, 38
High-speed cold rolling
An efficient thermal analysis for the prediction of minimum film thickness in inlet zone at high speed lubricated cold strip rolling, 238
High-temperature tensile properties
Reaction synthesis of Ni/Ni_3Al multilayer composites using Ni and Al foils: High-temperature tensile properties and deformation behaviour, 433
Hybrids
Hybrids for finishing cotton fabric with durable handle performance, 385

Impact damage
Micro-machinability of monocrystal silicon by direct etching using excimer laser, 390
Inconel 718
Tool life and surface integrity aspects when drilling and hole making in Inconel 718, 424
In-mould decoration
Mechanical properties of polymer films used in in-mould decoration, 221
Inorganic compounds
Thin film of bis(ethylenedithio)-tetrathiafulvalene radical salt with Dawson polyoxometalate, 153
Intermetallic composite
Fabrication of nickel aluminide intermetallic-alumina nanocomposite via reaction synthesis, 279
Intermetallics
Synthesis of nanocrystalline NiAl by mechanical alloying, 312
Internal oxidation
Properties of copper matrix reinforced with various size and amount of Al_2O_3 particles, 106

Kaolinitic–illitic clay
Effect of moisture content on extrusion process of kaolinitic–illitic clay in manufacturing of ceramic Raschig ring, 232

316L
Microinjection moulding of 316L/17-4PH and 316L/Fe powders for fabrication of magnetic–nonmagnetic bimetals, 259

L_{27} orthogonal array
Optimizing power consumption for CNC turned parts using response surface methodology and Taguchi's technique—A comparative analysis, 373
Large plastic strains
Numerical damage prediction in deep-drawing of sheet metals, 71
Liquid phase sintering
Toughened ZrO_2 ceramics sintered with a La_2O_3-rich glass as additive, 126
Loading effect
A three-dimensional model of the wire-arc spray process and its experimental validation, 94
Lobatto points
An efficient thermal analysis for the prediction of minimum film thickness in inlet zone at high speed lubricated cold strip rolling, 238
Low frequency
High-power low-frequency ultrasound: A review of tissue dissection and ablation in medicine and surgery, 38
LPG bottle
Numerical simulation and analysis on the deep drawing of LPG bottles, 416

Machine vision
Application of the structured illumination method for automated visual inspection of the loudspeaker cones, 59
Machining
Experimental and numerical study of machined aluminum tailor-made blanks, 288
Machining at both electrodes
On the mechanism of material removal in electrochemical spark machining of quartz under different polarity conditions, 460
Magnesium
FE analysis of metal flow and weld seam formation in a porthole die during the extrusion of a magnesium alloy into a square tube and the effect of ram speed on weld strength, 185
Magnetic–nonmagnetic
Microinjection moulding of 316L/17-4PH and 316L/Fe powders for fabrication of magnetic–nonmagnetic bimetals, 259
Magnetoplasmadynamic
Development and implementation of a magnetoplasmadynamic thruster for welding and cutting, 398
Martensitic transformation
Prediction of martensite and austenite start temperatures of the Fe-based shape memory alloys by artificial neural networks, 146
Mechanical alloying
Properties of copper matrix reinforced with various size and amount of Al_2O_3 particles, 106
Synthesis of nanocrystalline NiAl by mechanical alloying, 312
Mechanical properties
Toughened ZrO_2 ceramics sintered with a La_2O_3-rich glass as additive, 126
Mechanical properties of polymer films used in in-mould decoration, 221
Metal injection molding (MIM)
Fabrication of metal matrix composites by metal injection molding—A review, 12
Metal matrix composite (MMC)
Fabrication of metal matrix composites by metal injection molding—A review, 12
Microchannel
Cutting process of glass with inclined ball end mill, 356
Microfabrication
Study on the microfabrication technique by femtosecond laser two-photon photopolymerization, 158
Microhardness tests
Study of microstructure, phases and microhardness of metallic coatings deposited by flame thermal spray, 410
Micro-MIM
Microinjection moulding of 316L/17-4PH and 316L/Fe powders for fabrication of magnetic–nonmagnetic bimetals, 259

Microstructure
A comprehensive study of plastic deformation mechanism of the metallic materials by 'X-ray' computed tomography ('X-ray' CT), 133
Effect of moisture content on extrusion process of kaolinitic–illitic clay in manufacturing of ceramic Raschig ring, 232
Milling operation
Prediction of surface roughness profiles for milled surfaces using an artificial neural network and fractal geometry approach, 271
Minimum film thickness
An efficient thermal analysis for the prediction of minimum film thickness in inlet zone at high speed lubricated cold strip rolling, 238
Minimum quantity lubrication
Studies on minimum quantity lubrication (MQL) and air cooling at drilling, 339
Modification level
Identification and evaluation of modification level for compacted graphite cast iron, 471
Moisture content
Effect of moisture content on extrusion process of kaolinitic–illitic clay in manufacturing of ceramic Raschig ring, 232
Morphological structure
Physical–mechanical, superconducting, thermo-physical properties and interphase phenomena of polymer–ceramic nano-composites, 319
Morphology of worn surfaces
Three-body abrasive wear behaviour of particulate-filled glass–vinyl ester composites, 306
Multilayer composites
Reaction synthesis of Ni/Ni_3Al multilayer composites using Ni and Al foils: High-temperature tensile properties and deformation behaviour, 433

Nanocomposite
Fabrication of nickel aluminide intermetallic-alumina nanocomposite via reaction synthesis, 279
Nanostructured materials
Synthesis of nanocrystalline NiAl by mechanical alloying, 312
Neural network
Prediction of surface roughness profiles for milled surfaces using an artificial neural network and fractal geometry approach, 271
Ni_3Al
Reaction synthesis of Ni/Ni_3Al multilayer composites using Ni and Al foils: High-temperature tensile properties and deformation behaviour, 433
NiAl
Synthesis of nanocrystalline NiAl by mechanical alloying, 312
Non-Newtonian index
Shear and elongational flow properties of thermoplastic polyvinyl alcohol melts with different plasticizer contents and degrees of polymerization, 331
Non-thermal processing
Micro-machinability of monocrystal silicon by direct etching using excimer laser, 390

Orthogonal array
Experimental investigation on flow-forming of AA6061 alloy—A Taguchi approach, 283

Particle size
Effects of particle size of 8 mol% Y_2O_3 stabilized ZrO_2 (YSZ) and additive Ta_2O_5 on the phase composition and the microstructure of sintered YSZ electrolyte, 199
Pearlite
Pearlite determination in plain carbon steel by eddy current method, 316

17-4PH
Microinjection moulding of 316L/17-4PH and 316L/Fe powders for fabrication of magnetic–nonmagnetic bimetals, 259

Phase transformation
Effects of particle size of 8 mol% Y_2O_3 stabilized ZrO_2 (YSZ) and additive Ta_2O_5 on the phase composition and the microstructure of sintered YSZ electrolyte, 199
Photonic crystal
Study on the microfabrication technique by femtosecond laser two-photon photopolymerization, 158
Photopolymerization
Study on the microfabrication technique by femtosecond laser two-photon photopolymerization, 158
Piercing
The effect of using a sprung stripper in sheet metal cutting, 176
Plasma
Structural modifications of M35 steel submitted to thermal gradients in plasma reactor, 115
Development and implementation of a magnetoplasmadynamic thruster for welding and cutting, 398
Plastic anisotropy
Numerical damage prediction in deep-drawing of sheet metals, 71
Plastic deformation
A comprehensive study of plastic deformation mechanism of the metallic materials by 'X-ray' computed tomography ('X-ray' CT), 133
Plasticization
Shear and elongational flow properties of thermoplastic polyvinyl alcohol melts with different plasticizer contents and degrees of polymerization, 331
Polycarbonate
Mechanical properties of polymer films used in in-mould decoration, 221
Polyester
Mechanical properties of polymer films used in in-mould decoration, 221
Polymer
Physical–mechanical, superconducting, thermo-physical properties and interphase phenomena of polymer–ceramic nano-composites, 319
Powder injection molding (PIM)
Fabrication of metal matrix composites by metal injection molding—A review, 12
Powder metallurgy
Fuzzy rule-based prediction of hardness for sintered HSS components, 212
Fabrication of nickel aluminide intermetallic-alumina nanocomposite via reaction synthesis, 279
Powder-mixed dielectric
Electrical discharge machining using simple and powder-mixed dielectric: The effect of the electrode area in the surface roughness and topography, 250

Process modeling
A three-dimensional model of the wire-arc spray process and its experimental validation, 94
Processing parameters
Effect of welding parameters on mechanical and microstructural properties of AA6082 joints produced by friction stir welding, 364
Profile
A study on the cross-sectional profile of flat rolled wire, 325
Properties
Properties of copper matrix reinforced with various size and amount of Al_2O_3 particles, 106
Pulsed GMA welding
Prediction of bead geometry in pulsed GMA welding using back propagation neural network, 300

Quartz work-piece
On the mechanism of material removal in electrochemical spark machining of quartz under different polarity conditions, 460

Range sensing
Application of the structured illumination method for automated visual inspection of the loudspeaker cones, 59
Raschig ring
Effect of moisture content on extrusion process of kaolinitic–illitic clay in manufacturing of ceramic Raschig ring, 232
Regression model
Prediction of bead geometry in pulsed GMA welding using back propagation neural network, 300
Reinforced copper matrix
Properties of copper matrix reinforced with various size and amount of Al_2O_3 particles, 106
Residual stresses
Modelling of the residual state of friction stir welded plates, 25
Response surface
Fuzzy rule-based prediction of hardness for sintered HSS components, 212
Response surface methodology
Optimizing power consumption for CNC turned parts using response surface methodology and Taguchi's technique—A comparative analysis, 373
Reverse polarity
On the mechanism of material removal in electrochemical spark machining of quartz under different polarity conditions, 460
Rolling
A study on the cross-sectional profile of flat rolled wire, 325

Saturation magnetization
Fabrication of nickel aluminide intermetallic-alumina nanocomposite via reaction synthesis, 279
Semiconductors
Thin film of bis(ethylenedithio)-tetrathiafulvalene radical salt with Dawson polyoxometalate, 153
Shear failure
Experimental evaluation of strains in the tension–compression using a new tool geometry, X-Die, 1
Shear flow properties
Shear and elongational flow properties of thermoplastic polyvinyl alcohol melts with different plasticizer contents and degrees of polymerization, 331
Shear stress
Finite element analysis of thermal stress in magnetron sputtered Ti coating, 205
Sheet metal
The effect of using a sprung stripper in sheet metal cutting, 176
Sheet-metal forming
Experimental evaluation of strains in the tension–compression using a new tool geometry, X-Die, 1
Silicon
Micro-machinability of monocrystal silicon by direct etching using excimer laser, 390
Simulation
Numerical simulation and analysis on the deep drawing of LPG bottles, 416
Sintering
Effects of particle size of 8 mol% Y_2O_3 stabilized ZrO_2 (YSZ) and additive Ta_2O_5 on the phase composition and the microstructure of sintered YSZ electrolyte, 199
Effect of moisture content on extrusion process of kaolinitic–illitic clay in manufacturing of ceramic Raschig ring, 232
Microinjection moulding of 316L/17-4PH and 316L/Fe powders for fabrication of magnetic–nonmagnetic bimetals, 259
Solar reflectance
White anodized thermal control coating on LY12 aluminum alloy, 405
Solid-state bonding
FE analysis of metal flow and weld seam formation in a porthole die during the extrusion of a magnesium alloy into a square tube and the effect of ram speed on weld strength, 185
Speed
Prediction of surface roughness profiles for milled surfaces using an artificial neural network and fractal geometry approach, 271
Steady state
Modelling of the residual state of friction stir welded plates, 25
Stiff hand
Hybrids for finishing cotton fabric with durable handle performance, 385
Strain paths
Experimental evaluation of strains in the tension–compression using a new tool geometry, X-Die, 1
Strain signature
Experimental evaluation of strains in the tension–compression using a new tool geometry, X-Die, 1
Stress concentration
Experimental and numerical study of machined aluminum tailor-made blanks, 288
Stripper
The effect of using a sprung stripper in sheet metal cutting, 176
Structured illumination
Application of the structured illumination method for automated visual inspection of the loudspeaker cones, 59
Superconductivity
Physical–mechanical, superconducting, thermo-physical properties and interphase phenomena of polymer–ceramic nano-composites, 319
Surface finish
Cutting process of glass with inclined ball end mill, 356

Surface integrity
Tool life and surface integrity aspects when drilling and hole making in Inconel 718, 424
Surface quality
Electrical discharge machining using simple and powder-mixed dielectric: The effect of the electrode area in the surface roughness and topography, 250
Surface roughness
Evolutionary programming method for modeling the EDM parameters for roughness, 347
Surface roughness profile
Prediction of surface roughness profiles for milled surfaces using an artificial neural network and fractal geometry approach, 271

Taguchi method
Experimental investigation on flow-forming of AA6061 alloy—A Taguchi approach, 283
Taguchi technique
Optimizing power consumption for CNC turned parts using response surface methodology and Taguchi's technique—A comparative analysis, 373
Tailor-made blanks
Experimental and numerical study of machined aluminum tailor-made blanks, 288
Ta_2O_5
Effects of particle size of 8 mol% Y_2O_3 stabilized ZrO_2 (YSZ) and additive Ta_2O_5 on the phase composition and the microstructure of sintered YSZ electrolyte, 199
Temperature rise in inlet zone
An efficient thermal analysis for the prediction of minimum film thickness in inlet zone at high speed lubricated cold strip rolling, 238
Tensile properties
Influences of tool pin profile and welding speed on the formation of friction stir processing zone in AA2219 aluminium alloy, 163
Texture
Influence of texture and grain structure on strain localisation and formability for AlMgSi alloys, 77
Thermal analysis
Identification and evaluation of modification level for compacted graphite cast iron, 471
Thermal control coating
White anodized thermal control coating on LY12 aluminum alloy, 405
Thermal gradient
Structural modifications of M35 steel submitted to thermal gradients in plasma reactor, 115
Thermal spray
A three-dimensional model of the wire-arc spray process and its experimental validation, 94
Thermal stress
Finite element analysis of thermal stress in magnetron sputtered Ti coating, 205
Thermohydrodynamic lubrication
An efficient thermal analysis for the prediction of minimum film thickness in inlet zone at high speed lubricated cold strip rolling, 238
Thermomechanical modelling
Modelling of the residual state of friction stir welded plates, 25
Thermoplastic polyvinyl alcohol
Shear and elongational flow properties of thermoplastic polyvinyl alcohol melts with different plasticizer contents and degrees of polymerization, 331
Thin films
Thin film of bis(ethylenedithio)-tetrathiafulvalene radical salt with Dawson polyoxometalate, 153
Three-body abrasive wear
Three-body abrasive wear behaviour of particulate-filled glass–vinyl ester composites, 306
Ti coating
Finite element analysis of thermal stress in magnetron sputtered Ti coating, 205
Tissue
High-power low-frequency ultrasound: A review of tissue dissection and ablation in medicine and surgery, 38
Tomographic density (TD)
A comprehensive study of plastic deformation mechanism of the metallic materials by 'X-ray' computed tomography ('X-ray' CT), 133
Tool inclination
Cutting process of glass with inclined ball end mill, 356
Tool life
Tool life and surface integrity aspects when drilling and hole making in Inconel 718, 424
Tool pin profile
Influences of tool pin profile and welding speed on the formation of friction stir processing zone in AA2219 aluminium alloy, 163
Tool wear
Experimental evaluation of strains in the tension–compression using a new tool geometry, X-Die, 1

Ultrasound
High-power low-frequency ultrasound: A review of tissue dissection and ablation in medicine and surgery, 38

Variable blank holder force
Numerical simulation and analysis on the deep drawing of LPG bottles, 416

Wear
Analysis of wear in deep-drawing process of a cylindrical cup, 451
Weibull modules
Effect of moisture content on extrusion process of kaolinitic–illitic clay in manufacturing of ceramic Raschig ring, 232
Welding
Development and implementation of a magneto-plasmadynamic thruster for welding and cutting, 398
Welding parameters
Prediction of bead geometry in pulsed GMA welding using back propagation neural network, 300
Welding speed
Influences of tool pin profile and welding speed on the formation of friction stir processing zone in AA2219 aluminium alloy, 163
Wet-dry resistance
Preparation of geopolymer from fluidized bed combustion bottom ash, 265
Wire
A study on the cross-sectional profile of flat rolled wire, 325
Wire-arc process
A three-dimensional model of the wire-arc spray process and its experimental validation, 94

X-Die
Experimental evaluation of strains in the tension–compression using a new tool geometry, X-Die, 1

X-ray computed tomography (CT)
A comprehensive study of plastic deformation mechanism of the metallic materials by 'X-ray' computed tomography ('X-ray' CT), 133
XRD/EDS
Study of microstructure, phases and microhardness of metallic coatings deposited by flame thermal spray, 410
ZrO_2
Toughened ZrO_2 ceramics sintered with a La_2O_3-rich glass as additive, 126
Effects of particle size of 8 mol% Y_2O_3 stabilized ZrO_2 (YSZ) and additive Ta_2O_5 on the phase composition and the microstructure of sintered YSZ electrolyte, 199

ELSEVIER

Volume 200, Issues 1–3, 8 May 2008

Journal of Materials Processing Technology

www.elsevier.com/locate/jmatprotec

Contents

Experimental evaluation of strains in the tension–compression using a new tool geometry, X-Die 1
A. Andersson, P. Thilderkvist, M. Liljengren

Fabrication of metal matrix composites by metal injection molding—A review 12
H. Ye, X.Y. Liu, H. Hong

Modelling of the residual state of friction stir welded plates 25
A. Bastier, M.H. Maitournam, F. Roger, K. Dang Van

High-power low-frequency ultrasound: A review of tissue dissection and ablation in medicine and surgery 38
B.J. O'Daly, E. Morris, G.P. Gavin, J.M. O'Byrne, G.B. McGuinness

Application of the structured illumination method for automated visual inspection of the loudspeaker cones 59
C.W. Liao, J.C. Su, Y.R. Lin, Y.S. Tarng

Numerical damage prediction in deep-drawing of sheet metals 71
M. Khelifa, M. Oudjene

Influence of texture and grain structure on strain localisation and formability for AlMgSi alloys 77
K.O. Pedersen, O.-G. Lademo, T. Berstad, T. Furu, O.S. Hopperstad

A three-dimensional model of the wire-arc spray process and its experimental validation 94
R. Bolot, M.-P. Planche, H. Liao, C. Coddet

Properties of copper matrix reinforced with various size and amount of Al_2O_3 particles 106
V. Rajkovic, D. Bozic, M.T. Jovanovic

Structural modifications of M35 steel submitted to thermal gradients in plasma reactor 115
N.K.A.M. Galvão, B.L.S. Costa, M.W.D. Mendes, R.A. de Brito, C.F. Souza Jr., C. Alves Jr.

DOE applied to optimization of aluminum alloy die castings 120
G.O. Verran, R.P.K. Mendes, L.V.O.D. Valentina

Toughened ZrO_2 ceramics sintered with a La_2O_3-rich glass as additive 126
C. Santos, R.C. Souza, N. Almeida, F.A. Almeida, R.R.F. Silva, M.H.F.V. Fernandes

A comprehensive study of plastic deformation mechanism of the metallic materials by 'X-ray' computed tomography ('X-ray' CT) 133
E. Bayraktar, M.A. Gonzalez Garza, C. Bathias

Prediction of martensite and austenite start temperatures of the Fe-based shape memory alloys by artificial neural networks 146
O. Eyercioglu, E. Kanca, M. Pala, E. Ozbay

Thin film of bis(ethylenedithio)-tetrathiafulvalene radical salt with Dawson polyoxometalate 153
H. Ma, J. Peng, X. Gu, Z. Ding

Study on the microfabrication technique by femtosecond laser two-photon photopolymerization 158
M. Zhou, H.F. Yang, J.J. Kong, F. Yan, L. Cai

Influences of tool pin profile and welding speed on the formation of friction stir processing zone in AA2219 aluminium alloy 163
K. Elangovan, V. Balasubramanian

(Contents continued on page I)

0924-0136(20080508)200:1/3;1-G

(Contents continued from OBC)

The effect of using a sprung stripper in sheet metal cutting 176
G.J.A. Bing, J. Wallbank

FE analysis of metal flow and weld seam formation in a porthole die during the extrusion of a magnesium alloy into a square tube and the effect of ram speed on weld strength 185
G. Liu, J. Zhou, J. Duszczyk

Effects of particle size of 8 mol% Y_2O_3 stabilized ZrO_2 (YSZ) and additive Ta_2O_5 on the phase composition and the microstructure of sintered YSZ electrolyte 199
H. Zhao, X. Li, F. Ju, U. Pal

Finite element analysis of thermal stress in magnetron sputtered Ti coating 205
V. Chawla, R. Jayaganthan, R. Chandra

Fuzzy rule-based prediction of hardness for sintered HSS components 212
D. Chatterjee, G. Sutradhar, B. Oraon

Mechanical properties of polymer films used in in-mould decoration 221
C.O. Phillips, T.C. Claypole, D.T. Gethin

Effect of moisture content on extrusion process of kaolinitic–illitic clay in manufacturing of ceramic Raschig ring 232
M. Salehi, A. Salem

An efficient thermal analysis for the prediction of minimum film thickness in inlet zone at high speed lubricated cold strip rolling 238
P. Singh, R.K. Pandey, Y. Nath

Electrical discharge machining using simple and powder-mixed dielectric: The effect of the electrode area in the surface roughness and topography 250
P. Peças, E. Henriques

Microinjection moulding of 316L/17-4PH and 316L/Fe powders for fabrication of magnetic–nonmagnetic bimetals 259
P. Imgrund, A. Rota, A. Simchi

Preparation of geopolymer from fluidized bed combustion bottom ash 265
R. Slavik, V. Bednarik, M. Vondruska, A. Nemec

Prediction of surface roughness profiles for milled surfaces using an artificial neural network and fractal geometry approach 271
I.A. El-Sonbaty, U.A. Khashaba, A.I. Selmy, A.I. Ali

Fabrication of nickel aluminide intermetallic-alumina nanocomposite via reaction synthesis 279
R. Ismail, I.I. Yaacob

Experimental investigation on flow-forming of AA6061 alloy—A Taguchi approach 283
M.J. Davidson, K. Balasubramanian, G.R.N. Tagore

Experimental and numerical study of machined aluminum tailor-made blanks 288
A.A. Zadpoor, J. Sinke, R. Benedictus

Prediction of bead geometry in pulsed GMA welding using back propagation neural network 300
K. Manikya Kanti, P. Srinivasa Rao

Three-body abrasive wear behaviour of particulate-filled glass–vinyl ester composites 306
B. Suresha, G. Chandramohan

Synthesis of nanocrystalline NiAl by mechanical alloying 312
M.H. Enayati, F. Karimzadeh, S.Z. Anvari

Pearlite determination in plain carbon steel by eddy current method 316
S.H. Khan, F. Ali, A.N. Khan, M.A. Iqbal

Physical–mechanical, superconducting, thermo-physical properties and interphase phenomena of polymer–ceramic nano-composites 319
S.P. Davtyan, A.O. Tonoyan, C. Schick, A.A. Tataryan, A.G. Sargsyan

A study on the cross-sectional profile of flat rolled wire 325
M. Kazeminezhad, A. Karimi Taheri, A. Kiet Tieu

Shear and elongational flow properties of thermoplastic polyvinyl alcohol melts with different plasticizer contents and degrees of polymerization 331
C.-A. Lin, T.-H. Ku

Studies on minimum quantity lubrication (MQL) and air cooling at drilling 339
B. Tasdelen, T. Wikblom, S. Ekered

Evolutionary programming method for modeling the EDM parameters for roughness 347
Ö. Salman, M.C. Kayacan

Cutting process of glass with inclined ball end mill 356
T. Matsumura, T. Ono

Effect of welding parameters on mechanical and microstructural properties of AA6082 joints produced by friction stir welding 364
P. Cavaliere, A. Squillace, F. Panella

Optimizing power consumption for CNC turned parts using response surface methodology and Taguchi's technique—A comparative analysis 373
A. Aggarwal, H. Singh, P. Kumar, M. Singh

Hybrids for finishing cotton fabric with durable handle performance 385
N.A. Ibrahim, M.H. Abo-Shosha, H.M. Fahmy, Z.M. El-sayed, A.A. Hebeish

Micro-machinability of monocrystal silicon by direct etching using excimer laser 390
W. Yuan, B. Ma

Development and implementation of a magnetoplasmadynamic thruster for welding and cutting 398
I.G. Machado, R.T. Lermen

White anodized thermal control coating on LY12 aluminum alloy 405
W. Xiaohong, Q. Wei, C. Bo, J. Zhaohua, L. Weiqiang, H. Weidong

Study of microstructure, phases and microhardness of metallic coatings deposited by flame thermal spray 410
M.A. Bradai, N. Bounar, A. Benabbas, A. Ati

Numerical simulation and analysis on the deep drawing of LPG bottles 416
R. Padmanabhan, M.C. Oliveira, J.L. Alves, L.F. Menezes

Tool life and surface integrity aspects when drilling and hole making in Inconel 718 424
A.R.C. Sharman, A. Amarasinghe, K. Ridgway

Reaction synthesis of Ni/Ni_3Al multilayer composites using Ni and Al foils: High-temperature tensile properties and deformation behaviour 433
H. Wang, J. Han, S. Du, D.O. Northwood

Processing and properties of ultrafine-grain aluminium alloy 6111 sheet 441
R. Lapovok, I. Timokhina, P.W.J. McKenzie, R. O'Donnell

Analysis of wear in deep-drawing process of a cylindrical cup 451
A.R. Shahani, I. Salehinia

On the mechanism of material removal in electrochemical spark machining of quartz under different polarity conditions 460
V.K. Jain, S. Adhikary

Identification and evaluation of modification level for compacted graphite cast iron 471
X.J. Sun, Y.X. Li, X. Chen

Author index 481

Subject index 483